Boosting the conversion of CO_2 with biochar to clean CO in an atmospheric plasmatron: A synergy of plasma chemistry and thermochemistry

Hao Zhang[a,*], Qinhuai Tan[a], Qunxing Huang[a], Kaiyi Wang[a], Xin Tu[b,*], Xiaotong Zhao[a,c], Chunfei Wu[c], Jianhua Yan[a], Xiaodong Li[a]

[a] *State Key Laboratory of Clean Energy Utilization, Zhejiang University, Hangzhou 310027, China*

[b] *Department of Electrical Engineering and Electronics, University of Liverpool, Liverpool L69 3GJ, UK*

[c] *School of Chemistry and Chemical Engineering, Queen's University Belfast, Belfast BT7 1NN, UK*

* Corresponding authors:

zhang_hao@zju.edu.cn (H. Zhang)

xin.tu@liverpool.ac.uk (X. Tu)

Synopsis

The synergy of plasma chemistry and thermochemistry boosts significantly the conversion of CO_2 with biochar to clean CO.

Abstract

In this work, the conversion of CO_2 into O_2-free CO has been investigated in an atmospheric plasmatron via the reaction with biochar. The effects of biochar source, pyrolysis temperature for biochar preparation, and gas-solid reaction patterns (fixed bed and fluidized bed) on the reaction performance were evaluated under different feed flow rates. The underlying mechanisms were explored using *in-situ* optical emission spectroscopy focusing on understanding the role of plasma chemistry and thermochemistry in CO_2 conversion. The results revealed that the presence of both biochar and plasma significantly facilitate CO_2 conversion. In comparison to thermal CO_2 splitting, the plasmatron CO_2 + C process dramatically enhanced the CO_2 conversion from 0% to 27.1%. Walnut shell biochar prepared at relatively high pyrolysis temperatures favored CO_2 conversion due to a high carbon content. A fixed bed surprisingly provided remarkably better performance than a fluidized bed for the CO_2 + C reaction, benefiting from a prompt consumption of the generated O_2 by biochar. The high electron density achieved in the plasmatron (10^{15} cm^{-3}) allows for a high processing capacity, and the moderate electron temperature (1.1-1.5 eV) with enhanced vibrational energy (6300-8200 K) obtained stimulates the most efficient CO_2 activation routes through vibrational excitation. The relatively high rotational (gas) temperatures in the core plasma area (2100-2400 K) and in the gas-solid reaction region (<1573 K) detrimentally drive the reverse reactions of CO_2 splitting, while advantageously boost the biochar-involved reactions respectively by thermochemistry. The synergy of plasma-chemistry-dominated CO_2 dissociation and the thermochemistry-dominated CO_2+C and O_2+C reactions accounts for the high CO_2 conversion obtained in the plasmatron CO_2+C process. The immediate study

provides a novel route for efficient CO_2 conversion by coupling plasma chemistry and thermochemistry.

Keywords: CO_2 conversion, biochar, plasmatron, plasma chemistry, thermochemistry

Introduction

Mitigation of greenhouse gas (GHG) emissions has been of unprecedented importance due to the increasingly severe global climate change crisis. In this context, recent research has intensified efforts to re-use and convert CO_2 as a viable feedstock into added-value products (*e.g.*, CO, methanol, methane, formaldehyde, and dimethyl ether) [1-4]. Nevertheless, due to the high stability of CO_2 molecule, its conversion to more reduced carbon products is thermodynamically unfavorable and requires a large amount of energy input [5]. For instance, a high temperature of up to 3500K is required to achieve a CO_2 conversion of 60-80%, with an equivalent efficiency of only around 50% and energy cost of up to 602 kJ/mol [6, 7]. A variety of CO_2 conversion routes are being investigated, including electrochemical, thermochemical, photochemical, biochemical, and catalytic conversion. Nevertheless, the distinctive downsides of these routes such as low conversion, limited productivity, lack of efficient and cost-effective catalyst, and/or sluggish kinetics limit their potential applications on a large scale [7, 8].

In this regard, atmospheric non-thermal plasma (NTP) processes have emerged as a promising alternative for CO_2 conversion [7, 9-12]. In NTPs, electrical energy is selectively applied to producing energetic electrons, typically of 1-10 eV [13]. These highly energetic electrons could activate the CO_2 molecules by excitation, ionization, and dissociation, producing a cascade of reactive species such as excited species, ions, molecules, and radicals that can initiate and further propagate reactions, without overheating the gas [9, 14, 15]. This behavior enables the thermodynamically unfavorable CO_2 conversion reaction to occur with reduced energy costs at atmospheric pressure. Importantly, high reaction rate and rapid start-up of NTP processes, in combination with the compactness, ease of installation, and flexibility,

enable direct utilization of electricity from intermittent renewable sources (*e.g.*, solar and wind), offering a flexible solution for peak shaving and grid stabilization [7, 9]. Consequently, increasing efforts have been focused on NTP-assisted CO_2 conversion into CO, hydrocarbons (*e.g.*, CH_4), and liquid chemicals (*e.g.*, methanol, formic acid), by using different types of NTPs such as gliding arc discharge (GAD), dielectric barrier discharge (DBD), microwave discharge (MW), and radio frequency (RF) discharge [7, 9-12, 16-21].

Among these studies, CO_2 splitting into CO is highly explored, since CO is a valuable chemical feedstock for synthesizing a range of fuels and chemicals [22]. However, CO_2 splitting is typically observed having a trade-off between the CO_2 conversion and energy efficiency in different types of NTPs. Among NTPs, warm plasmas such as GAD and MW provide relatively high gas temperature and energy density. The energy efficiency of warm plasma can be up to 35-40%. They also facilitate higher processing capacity, and their energy distribution stimulates the most efficient CO_2 decomposition route through vibrational excitation, whereas normally a low CO_2 conversion is obtained (*e.g.*, <20%) [7, 9, 12, 16, 17, 21, 23, 24]. In other NTPs such as DBD, a relatively higher CO_2 conversion of up to 50% was reported, whereas the energy efficiency is normally only <10% with significantly lower processing capacity [7, 9, 12, 25, 26]. Also, cost-effective separation of CO and O_2 is highly challenging. To enable a thermodynamically more favorable conversion of CO_2, the addition of H-containing co-reactants, *e.g.*, H_2 and CH_4, is commonly employed, producing syngas, hydrocarbons, or oxygenates (*e.g.*, acetic acid, methanol, ethanol, acetone, and formaldehyde) etc. [10, 18, 27]. High selectivity towards selected products with relatively high CO_2 conversion has been reported by using plasma catalysis. For instance, in a DBD plasma catalytic study of CO_2

hydrogenation to methane, Ahmad et al. reported a CO_2 conversion of up to 60% with a CH_4 selectivity of >97% [28]. Nevertheless, the requirement for H_2 and CH_4 sources and the resulting possible extra CO_2 generation severely limit the potential application of these processes. Also, the high complexity of the products caused by uncontrolled side reactions necessitates a product separation step before the target products can be further utilized. However, costly separation is known as one of the major barriers for the application of NTP assisted CO_2 conversion processes [10, 29, 30].

The intrinsic drawbacks of the above-mentioned NTP processes are motivating efforts towards more efficient routes for CO_2 conversion. In our previous work, biochar was used as the co-reactant for CO_2 conversion *via* the Boudouard reaction (Eq. (1)), which has been preliminarily explored for the first time in NTPs by using a specially designed atmospheric plasmatron [20]. In comparison to other H_2-containing co-reactants that are high-grade fuels, biochar is apparently more favored since it is easily derived from the carbonization of renewable biomass, fitting in the Cradle-to-Cradle concept [31-33]. The reaction of CO_2 plasma with coconut shell biochar exhibited a relatively high CO_2 conversion of ~21.3% and high CO concentration in the gas products of ~34.1% contributed by the Boudouard reaction, with favorably ultra-low O_2 concentration of <0.1% in the gas products [20]. Therefore, it allows for a conversion of CO_2 into O_2-free fuel gas in a catalyst-free plasma process, which potentially eliminates the need for a costly gas separation step. These explorative results indicate that the plasmatron assisted CO_2 reaction with biochar is a promising alternate for CO_2 utilization. Nevertheless, little is still known about the underlying mechanisms, and further significant efforts are also needed for performance optimization.

$CO_2 + C \rightarrow 2CO$ $\Delta H = 172.5$ kJ/mol (1)

The performance of CO_2 conversion in thermal catalytic Boudouard reaction is largely dependent on various factors such as the biochar properties and residence time [31, 34-39]. Therefore, in the present study, parameter studies have been performed to investigate the effects of biochar source (walnut shell, sawdust, rice straw), pyrolysis temperature (673, 773, 873K), and CO_2 feed flow rate (2-8 L/min) on the CO_2 conversion performance in the atmospheric plasmatron. The plasmatron favorably provides an extended 3D afterglow area with an appreciable volume outside the electrode, which also allowed us to test the implementation of different patterns for effective gas-solid reaction, *i.e.*, fixed bed and fluidized bed, without affecting a stable generation of plasma between the electrodes. Furthermore, NTPs with relatively high gas temperature (*e.g.*, >1500K) have the potential of driving reactions thermodynamically in addition to the plasma reactions, which, however, has been only scarcely investigated in gas conversion processes [40]. Another focus of this work is thus on understanding the role of plasma chemistry and thermochemistry in the conversion of CO_2 in the studied plasmatron chemical process. To this end, *in-situ* optical emission spectroscopy (OES) was employed to characterize the plasma in terms of electron density, electron temperature, vibrational temperature, and rotational (gas) temperature to obtain new insights on the reactions steered by different mechanisms. Moreover, to our knowledge, for the first time, the overall density of O atom was calculated based on the collected spectra, in a NTP assisted CO_2 splitting process. These obtained plasma parameters also provide a valuable basis for further modeling work.

Experimental setup and methods

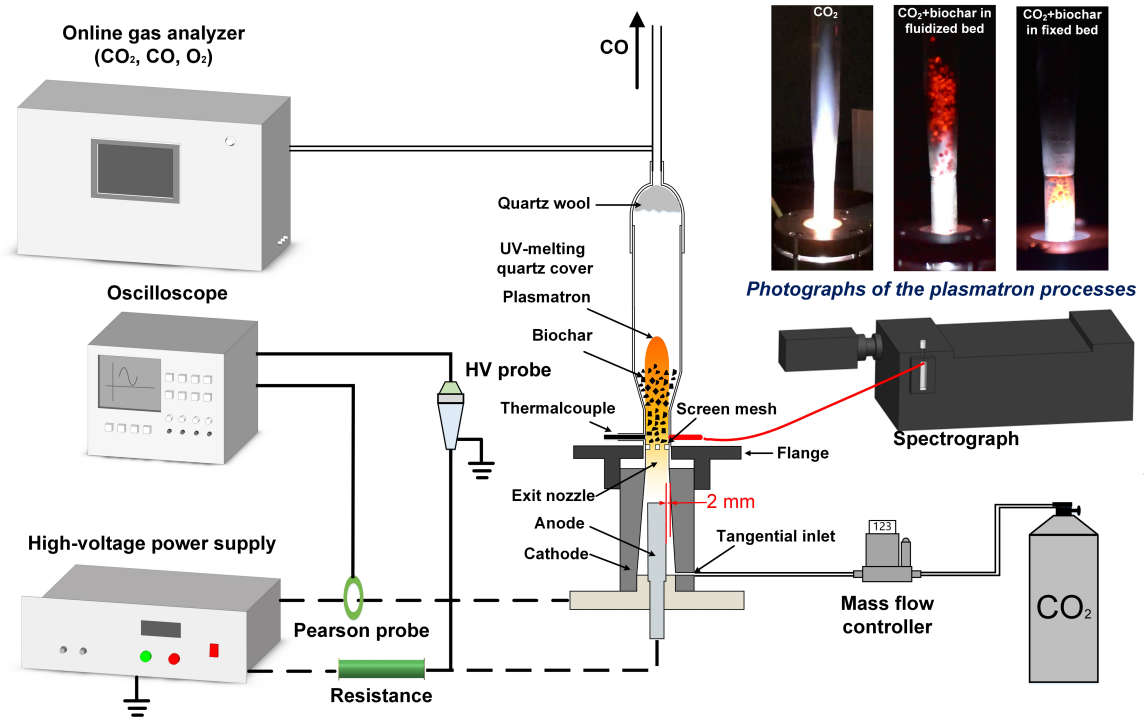

Fig. 1. Schematic diagram of the experimental setup. Photographs of the plasmatron processes without biochar (CO_2), and with biochar in the fluidized bed and fixed bed systems are displayed in the top-right panel.

A schematic diagram of the experimental setup is shown in Fig. 1. The homemade plasmatron reactor consists of a cylindrical inner anode and a convergent nozzle shaped outer cathode (grounded. Both electrodes are made of stainless steel. The anode was powered by a customized 10 kV DC power supply (TLP2040, Teslaman) that was operated at the constant-voltage mode in the experiments. A 40 kΩ resistance was connected in series in the circuit to limit and stabilize the discharge current. The feed gas CO_2 (99.99% purity) was injected through a tangential inlet at the bottom of the cathode to form a swirling flow inside the reactor for plasmatron generation, with the flow rate controlled by a mass flow controller (MFC, YJ-700C). After being initiated at the narrowest gap point (2 mm) between the electrodes, the arc was

pushed downstream while it rotated rapidly around the anode, and the formed plasma gas then extended from the convergent exit nozzle to form a large 3D torch-like plasmatron outside the electrode region. A quartz cover with a gas exit on the top was assembled downstream of the electrode region to form an enclosed plasmatron reaction area.

In the experiments with the presence of biochar, a screen mesh (openings with 1 mm diameter) was assembled inside the quartz cover at ~10 mm above the exit nozzle to serve as the biochar bed for gas-solid reaction. After passing through the openings of the screen mesh, the formed plasma was split into numerous micro plasma jets, providing both significant numbers of plasma reactive species and heat for the gas-solid CO_2 reaction with biochar on the mesh. In the fixed bed pattern, a quartz rod was placed on the top of biochar to fix the particles, whereas in the fluidized bed pattern, the quartz rod was absent, and thus a gas-solid fluidization region could be formed with the help of the high-speed CO_2 plasma flow. A plug of quartz glass wool was placed at the exit of the quartz cover to block any biochar particles.

The biochar used in this work was prepared by the carbonization of the raw biomass materials following commonly used procedures [41-43]. Three commercial biomass materials, including sawdust, rice straw, and walnut shell (Zhengjie Environmental Protection Technology Co., Ltd) were employed. The biomass samples were first pulverized to 2~3 mm, and then dried at 353K for 24 h before they were carbonized in a tubular furnace (SKF-2-13, LTYQ, China). For each batch, the pre-treated biomass samples were heated from room temperature to the set temperature of 673, 773, or 873K at a heating rate of 10°C/min, and then kept at the set temperature for 3 h under nitrogen atmosphere (99.99%, 150 mL/min). After carbonization, the

samples were cooled naturally to room temperature without stopping the nitrogen flow. Finally, the collected biochar was ground to around 1 mm for experiments. 1g of biochar sample was used in each experiment. Proximate and ultimate analyses of the biochar were conducted in a 5E-MAG6700 industrial analyzer and a 5E-CHN2000 elemental analyzer, respectively.

Previous analyses have shown that CO_2, CO, and O_2 are the dominant products, with only <0.06 % H_2 and < 0.01% CH_4, in the presence of biochar [20]. Therefore, only the concentrations of CO_2, CO, and O_2 were measured in this work by using an online gas analyzer (UE-50, ONUEE, uncertainty: ±0.1%) that equipped with non-dispersive infrared (NDIR) sensors for CO_2 and CO, and electrochemical sensor for O_2 (temporal resolution of 2s). In the CO_2 decomposition process without biochar, the data were collected only when a stable gas composition was observed (typically >90s after plasma-on), whereas in the process with biochar, the minimum CO_2 concentrations, together with the corresponding O_2 and CO concentrations, were used (typically >30s after plasma on). Each experiment was repeated three times and the mean values with error bands are given in the figures.

Plasma gas temperature is a critical factor affecting the plasma chemical process. The temperature in the biochar bed region was therefore measured under the studied conditions by using a S-type Pt-Rh thermocouple placed 10 mm vertically above the screen mesh inside the quartz cover. The temperature was recorded only after a relatively stable value was observed with a fluctuation of within 20K (<2%), meaning the reaction was already stabilized after plasma-on. An uncertainty of 50K is expected for the temperature measurement.

Moreover, to obtain new insights into the electron energy distribution of the plasma as well as the intermediate species formed, *in-situ* OES study has been performed for selected conditions. The emission spectrum of the plasma was recorded by using a monochromator (PI-Acton 2750, 750 mm, grating: 1200 grooves/mm and 2400 grooves/mm). An optical fiber was placed ~30 mm above the exit of the quartz cover to collect the overall spectra of the plasma region. Only the conditions in the absence of biochar were investigated in the OES study, due to limited visualisation in the presence of biochar.

The reaction performance was evaluated mainly in terms of CO_2 conversion (X_{CO2}) and energy efficiency (η), as defined below.

$$X_{CO_2}(\%)=\frac{Q_{in}(\text{mol/min})-Q_{out}(\text{mol/min})\times C_{(CO_2\ out)}(\%)}{Q_{in}(\text{mol/min})}\times 100\% \quad (2)$$

where Q_{in} and Q_{out} are the inlet and outlet total flow rates, respectively; $C_{(CO_2\ out)}$ is the CO_2 concentration in the outlet gas. To take the gas expansion effect into account [20, 21, 44]. Q_{out} was calculated based on the oxygen balance of the gas stream before and after the reactions.

$$Q_{out}(\text{mol/min})=\frac{2\times Q_{in}(\text{mol/min})}{2\times\left[C_{(CO_2\ out)}(\%)+C_{(O_2\ out)}(\%)\right]+C_{(CO\ out)}(\%)} \quad (3)$$

where $C_{(O2\ out)}$ and $C_{(CO\ out)}$ are the concentrations of O_2 and CO in the outlet gas. To verify this method, a film flow meter (Sensidyne Gilibrator-2) was used to simultaneously measure the outlet gas flow rate of several additional experiments. The results were compared with those obtained by the proposed oxygen-balance method (Eq. (3)), and are given in Table S1 in the Supporting Information (SI). As can be seen, the deviation of the obtained flow rates between the two methods is only within 2%, demonstrating the plausibility of the proposed oxygen-

balance method. In the final experiments, the oxygen-balance method was used instead of the direct measurement method to avoid any pressure drop in the gas lines caused by using the film flow meter.

Energy efficiency (η) of the reaction system is defined as the ratio of the standard reaction enthalpy ΔH to the power consumption of the process, following the typical definition for plasma CO_2 conversion processes [7].

$$\eta(\%)=\frac{X_{CO_2}(\%)\times Q_{in}(\text{mol/min})\times \Delta H\ (\text{kJ/mol})}{\text{Discharge power (W)}\ \times\ 60/1000}\times 100\% \quad (4)$$

where ΔH = 280 kJ/mol for the pure CO_2 decomposition reaction [7]. Nevertheless, for the reaction of CO_2 with biochar, both the CO_2 decomposition and Boudouard reactions potentially exist. In this case, the ΔH was calculated according to the respective contributions of the two net reactions to CO_2 conversion (α_{Dec}, α_{Bou}):

280 (kJ/mol) × α_{Dec} + 172.5 (kJ/mol) × α_{Bou}. Since the O_2 in the gas products is formed theoretically exclusively from the CO_2 decomposition reaction, α_{Dec} and α_{Bou} can then be calculated based on the oxygen balance, as shown in Eq. (5) and Eq. (6).

$$\alpha_{Dec}\ (\%)=\frac{2C_{(O_2\ out)}(\%)}{2C_{(O_2\ out)}(\%)+1/2\times(C_{(CO\ out)}(\%)-2C_{(O_2\ out)}(\%))} \quad (5)$$

$$\alpha_{Bou}\ (\%)=\frac{1/2(C_{(CO\ out)}(\%)-2C_{(O_2\ out)}(\%))}{2C_{(O_2\ out)}(\%)+1/2\times(C_{(CO\ out)}(\%)-2C_{(O_2\ out)}(\%))} \quad (6)$$

Specific energy input (SEI) was defined to represent the energy density applied to the plasma processes, and that of different studied conditions in this work is given in Fig. S1 in SI.

$$SEI\,(\text{kJ/L})=\frac{\text{Discharge power (W)}\times 60/1000}{Q_{in}(\text{mol/min})/22.4} \quad (7)$$

The experimental conditions studied in this work are tabulated in Table 1.

Table 1. The plasma experimental conditions studied in this work

No.	CO_2 flow rate (L/min)	Biochar type	Pyrolysis temperature for biochar preparation (K)	Type of the biochar bed
1	2-8	Without biochar	/	/
2	2-8	Walnut shell, Sawdust, Rice straw	773	Fixed bed
3	2-8	Walnut shell	673, 773, 873	Fixed bed
4	2-8	Walnut shell	773	Fluidized bed

Results and discussions

In this section, the effect of plasma and biochar on the conversion of CO_2 will be analyzed first by comparing the performance of CO_2 conversion with/without biochar in the traditional thermal process and in the plasmatron process (Section 3.1). The effect of biochar characteristics on CO_2 conversion will be presented in Section 3.2 in terms of biochar type and pyrolysis temperature for biochar preparation. The combination of plasmatron with two gas-solid reaction patterns, *i.e.*, fixed bed and fluidized bed, will be compared and discussed in Section 3.3. Finally, the underlying mechanisms will be proposed in Section 3.4, based on the experimental observations and the electron energy distribution information obtained from the

OES results, with a focus on understanding the interaction of plasma chemistry and thermochemistry.

Effect of plasma and biochar on CO_2 conversion. To elucidate the effect of plasma on CO_2 conversion, thermal experiments have been additionally performed in a tubular furnace at 1273K (comparable to that in the plasmatron, refer to Fig. 8), studying both CO_2 decomposition and CO_2 reaction with biochar. The biochar was derived from the pyrolysis of the walnut shell (~1 mm in diameter) at 773K. The residence time of CO_2 in the reaction region was similar for both the thermal and plasmatron experiments. The results of CO_2 conversion and energy efficiency upon increasing feed CO_2 flow rate are plotted in Fig. 2. Note that due to the different definitions in thermal and plasma processes, the energy efficiency of the thermal processes was not given for comparison in Fig. 2(b). As seen from Fig. 2(a), decomposition of CO_2 in the absence of biochar cannot be thermally stimulated by a similar gas temperature level with that in the plasmatron under the studied flow rates. The addition of biochar into CO_2 drives slightly the conversion of CO_2 but only when the furnace temperature reaches up to 900°C (CO_2 conversion = 0.12%, see Fig. S2 in SI). A maximum CO_2 conversion of only 5.3% can be reached in the thermal CO_2 + C reaction at the lowest feed flow rate of 2 L/min (at 1273K).

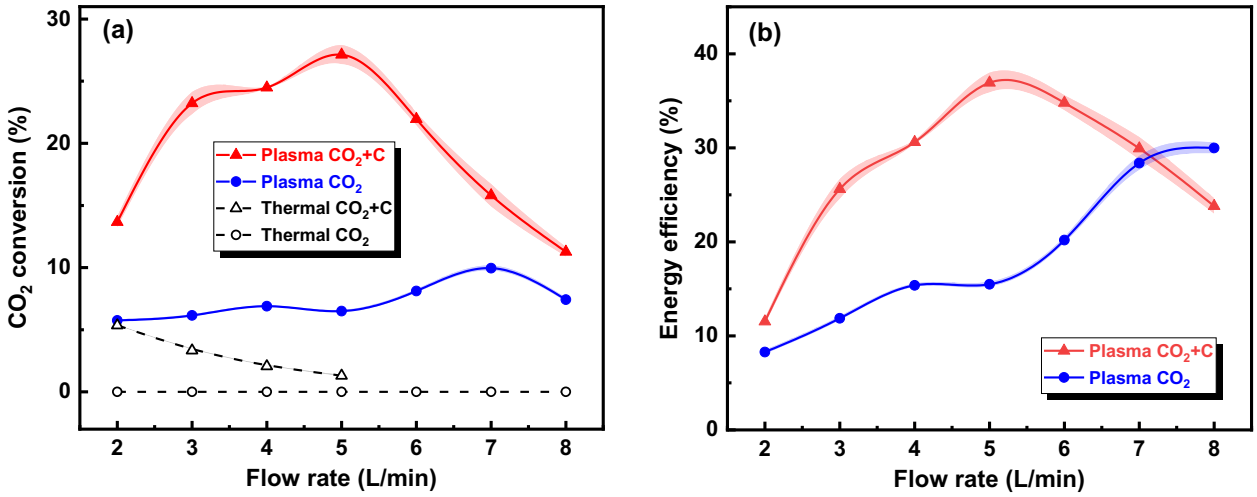

Fig. 2. CO_2 conversion (a) and energy efficiency (b) as a function of CO_2 flow rate in the CO_2 decomposition reaction and CO_2 reaction with biochar in the thermal and plasmatron processes. Results for the thermal processes were obtained in a tubular furnace at 1273K.

In the plasma CO_2 decomposition process, a maximum CO_2 conversion of up to 10.0% was obtained at a flow rate of 7 L/min, while the energy efficiency reaches 28.4%. The addition of biochar into CO_2 plasma improved the CO_2 conversion and energy efficiency, especially at relatively low flow rates of $\leqslant$6 L/min. For instance, at flow rate = 5 L/min, the CO_2 conversion and energy efficiency were increased by a factor of 4 and 2.5, respectively, in comparison to the plasma reaction without biochar, reaching up to 27.1% and 36.9%. The presence of biochar promotes a more efficient conversion of CO_2 conceivably *via* either directly the Boudouard reaction between CO_2 and C (Eq. 1) or the consumption of O_2 by C that favors the forward reaction of CO_2 decomposition. Therefore, it is very clear that, the presence of plasma facilitates the conversion of CO_2 in the reactions of both with and without biochar, compared to thermal route.

The observed conversion of CO_2 in the thermally driven CO_2 + C reaction at 1273K (⩽5.3%, see Fig. 2(a)) indicates that the thermochemistry can highly likely contribute to CO_2 conversion. This can be the case as well in the plasmatron assisted CO_2 reaction with biochar, because the gas temperature was comparable with the thermally driven or even higher (up to 1240-1570K, refer to Fig. 8). In addition to that, as shown in Fig. 2, when used the plasmatron, the CO_2 conversion increases from 0% to 10% at flow rate = 7 L/min in the CO_2 decomposition reaction, and that in the CO_2 + C reaction even increases from 1.3% to 27.1% at flow rate = 5 L/min. This indicated that in addition to the thermochemistry due to high gas temperature, the plasma chemistry also has significant role and contribute towards the overall CO_2 conversion. Particularly, its contribution could be more with the feed flow rate (⩾ 4 L/min) due to the decreasing gas temperature (and thus thermochemistry) (see Fig. 8), corroborated by observation in Fig. 2(a). The observation is that, CO_2 conversion shows a declining trend in the thermal process but a rising trend in the plasmatron process between flow rates of 2 and 5 L/min. Nevertheless, the cascade effect of plasma chemistry and thermochemistry could not be ignored and their interaction is essential for an efficient conversion of CO_2 in the plasmatron assisted CO_2 reaction with biochar. Detailed discussions on the underlying mechanisms will be presented in Section 3.4.

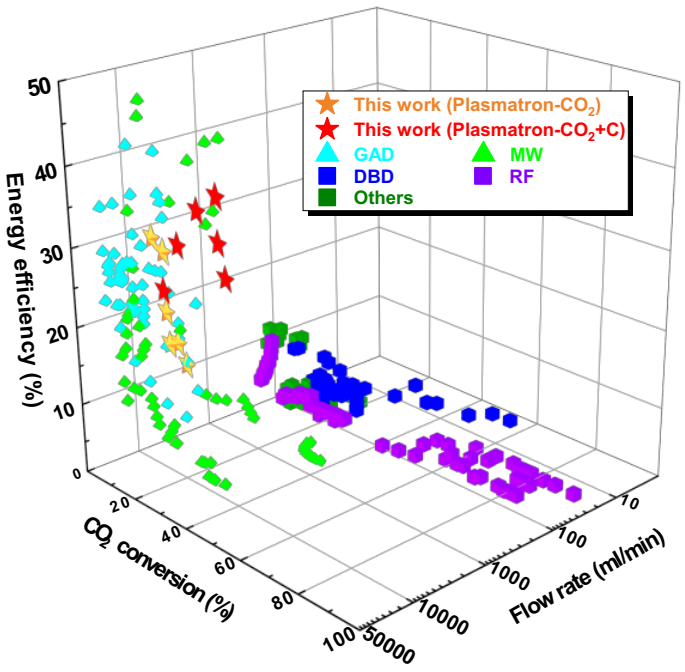

Fig. 3. Experimental data collected from the literature for CO_2 splitting in different NTPs, including GAD [22, 23, 45-48], MW [49-54], DBD [55-61], RF [62, 63] and others [64-67], together with the results of CO_2 splitting and CO_2 + biochar reaction obtained in the atmospheric plasmatron in this work.

The performance of the studied plasmatron assisted CO_2 conversion reactions is compared with those obtained in other typical NTPs reported for CO_2 splitting, in terms of CO_2 conversion, energy efficiency, and processing capacity (feed CO_2 flow rate), as shown in Fig. 3. As can be seen, typical NTPs such as DBD, RF discharge, and corona can potentially provide high CO_2 conversions of up to 90%, but only when the feed CO_2 flow rate is very limited (*e.g.*, 15 ml/min), yielding an energy efficiency of only below 10%, and are therefore not competitive from the viewpoint of industrial application. In comparison, despite a normally relatively low CO_2 conversion, high energy efficiency (*e.g.*, 40%) and processing capacity (*e.g.*, 10 L/min) can be achieved in the so-called "warm plasmas" [7, 16, 40] such as GAD, MW, and the

plasmatron in this work (as evidenced from the OES study in Section 3.4). Nevertheless, upon the addition of biochar, the plasmatron assisted CO_2 + C process to some extent breaks the trade-off between CO_2 conversion and energy efficiency and exhibits better overall performance. Considering the benefit of generating the O_2-free fuel gas (CO) that could eliminate the need for a costly gas separation step [20], the atmospheric plasmatron assisted CO_2 + biochar process shows promising application prospects for CO_2 utilization. Nevertheless, further enhancement of the CO_2 conversion performance is still necessary and can be expected by optimizing the reactor design and operating conditions (see more discussions in Section 3.4).

Effect of biochar properties. In this section, three types of biochar obtained from the walnut shell, sawdust, and rice straw (pyrolysis temperature = 773K), as well as the walnut shell biochar prepared at different pyrolysis temperatures of 673K, 773K, and 873K, have been tested for the plasmatron assisted CO_2 + C reaction, to investigate the influence of the biochar properties. The results upon increasing feed flow rate are presented in Fig. 4 and Fig. 5. To elucidate the link between the biochar property and the reaction performance, proximate and ultimate analyses of the biochar have been performed, and the results are tabulated in Table 2 and Table 3, respectively.

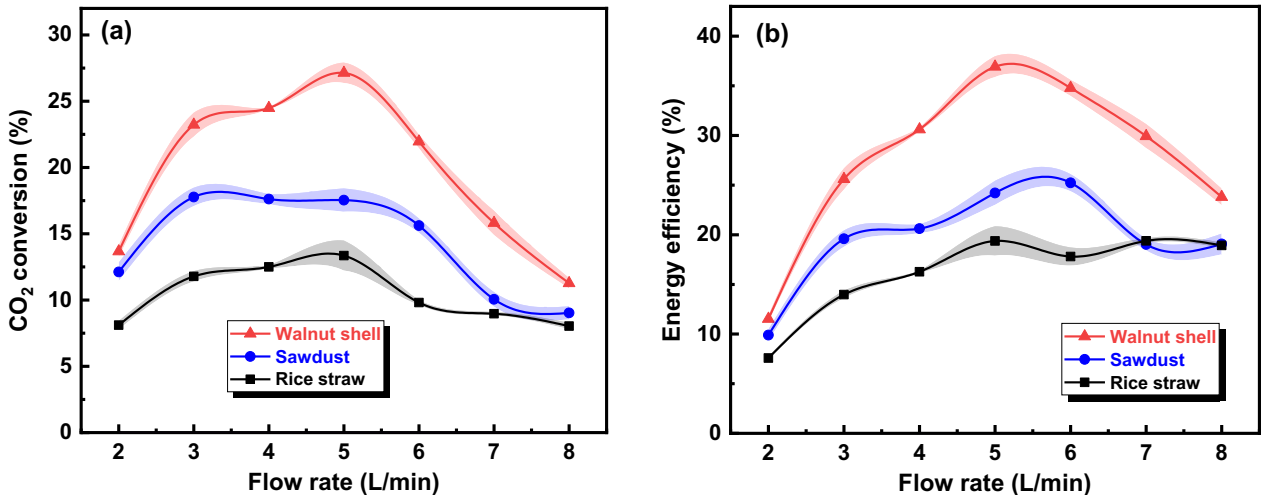

Fig. 4. CO_2 conversion (a) and energy efficiency (b) as a function of CO_2 flow rate in the plasmatron assisted CO_2 reactions with walnut shell biochar, sawdust biochar, and rice straw biochar, respectively. Pyrolysis temperature = 773K.

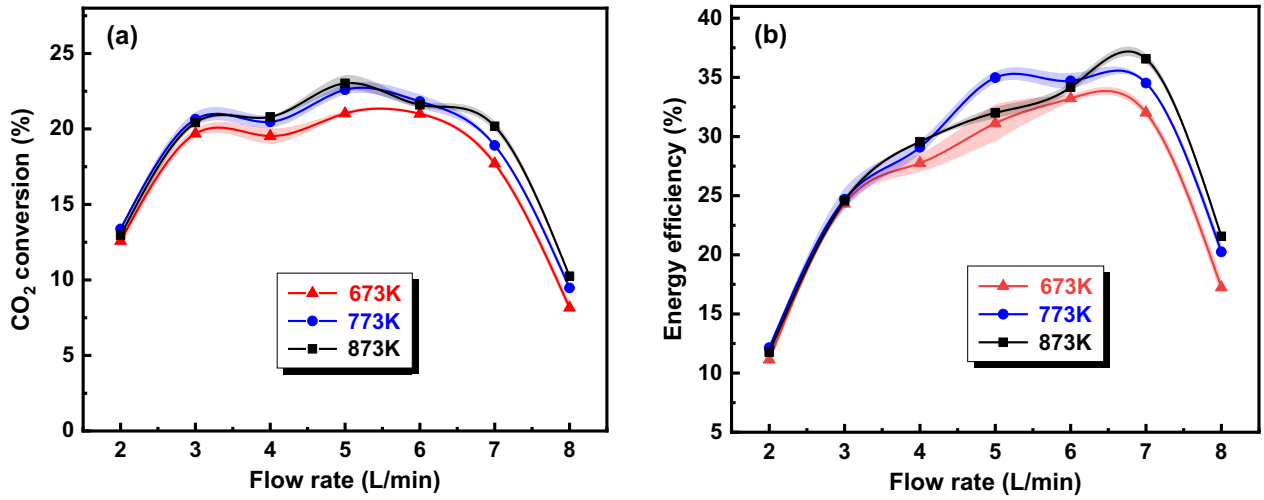

Fig. 5. CO_2 conversion (a) and energy efficiency (b) as a function of CO_2 flow rate in the plasmatron assisted CO_2 reaction with walnut shell biochar prepared at pyrolysis temperatures of 673K, 773K, 873K, respectively.

Table 2. Proximate and ultimate analysis of the different types of biochar

	Proximate analysis (wt.%)				Ultimate analysis (wt.%)				
Type	Water	Ash	Volatiles	Fixed carbon	C	H	O	N	S

Walnut shell	2.28	3.81	11.02	82.89	84.13	3.24	6.24	0.25	0.05
Sawdust	5.93	4.63	8.93	80.51	75.36	2.43	10.3	1.27	0.08
Rice straw	2.29	26.22	9.24	62.25	62.38	2.29	6.04	0.35	0.43

Table 3 Proximate and ultimate analysis of the walnut shell biochar prepared at different pyrolysis temperatures.

	Proximate analysis (wt.%)				**Ultimate analysis (wt.%)**				
Temperature	**Water**	**Ash**	**Volatiles**	**Fixed carbon**	**C**	**H**	**O**	**N**	**S**
673K	3.41	1.09	17.80	77.7	82.02	3.00	10.30	0.15	0.05
773K	3.26	1.66	10.38	84.7	86.04	2.69	6.17	0.18	0.06
873K	3.17	2.65	5.83	88.35	87.97	2.04	3.94	0.23	0.08

As can be observed, upon rising feed flow rate, the CO_2 conversion and energy efficiency increase first to a peak at flow rates of around 5-7 L/min and then decrease or flatten, for all the cases with different types of biochar. The initial rise of CO_2 conversion (and energy efficiency) could be attribted to the increasing gas temperature (see Fig. 8 in Section 3.3) that thermally favors the endothermic conversion of CO_2. Another factor to be considered is the decreased residence time of CO_2 in plasma with a rising flow rate, which likely weakens the contribution of the reactions for CO_2 re-formation, *e.g.*, CO + O, CO + O_2 [11, 23]. The later decrease of CO_2 conversion is likely due to a combined effect of the decreased SEI (see Fig. S1 in SI), decreased residence time, and decreased gas temperature (see Fig. 8 in Section 3.3), which globally weakens both the forward and reverse reactions of CO_2 conversion by both

plasma chemistry and thermochemistry, to different extents. As shown above in Fig. 2, the CO_2 conversion in the plasma CO_2 + C case peaks at a lower flow rate in comparison to the plasma CO_2 decomposition case. This could be related to the higher contribution of the thermal chemistry in the plasma CO_2 + C process, which is then retarded upon a descending gas temperature.

As clearly observed from Fig. 4, walnut shell biochar gives rise to apparently more efficient conversion of CO_2 in comparison to sawdust and rice straw, with a maximum CO_2 conversion twice that of rice straw. Table 2 shows that the walnut shell biochar has the highest carbon content (84.13%), followed by sawdust (75.36%) and then rice straw (62.38%). As expected, a higher carbon content (or fixed carbon fraction) in the biochar favors the conversion of CO_2, due to the decisive role of carbon in the CO_2 + C reaction. The effect of pyrolysis temperature on the biochar reactivity is largely less pronouncedly, whereas the above conclusion still applies. As shown in Fig. 5, the 773K- and 873K-prepared biochars with slightly higher carbon content (and fixed carbon fraction) exhibit slightly better performance in terms of both CO_2 conversion and energy efficiency. In addition, in the conventional thermal CO_2 + biochar process, a positive effect of a higher volatile fraction on the biochar reactivity was reported due to the enhanced concentration of active sites in the char matrix during devolatilization [68, 69]. Nevertheless, no convincingly clear correlation is noted between the volatile fraction and the CO2 conversion performance in this study. For example, the rice straw biochar (Table 2) or the 673K-prepared walnut shell (Table 3) does not consistently provide higher CO_2 conversion than other cases with lower volatiles. Also, the increase of pyrolysis temperature for biochar in conventional thermal CO_2 + C reactions was noted to decrease the reactivity of biochar, due to

the ordering of carbon matrix and declining of the active site concentration [70, 71]. This is again not seen in the plasmatron assisted CO_2 reaction with biochar in this study. The above phenomena indicate that the active-site-dependent mechanism that is dominant in a thermal CO_2 + biochar process [72, 73] does not apply to the plasmatron process, where plasma chemistry (or the combination with thermochemistry) plays an essential role. These results allow us to make a plausible conclusion that the carbon content in biochar is one of the most decisive and limiting factors for CO_2 conversion in the plasmatron assisted CO_2 reaction with biochar. And, in the following sections, the walnut shell biochar is consistently used, given its better performance exhibited for CO_2 conversion. Additional information on the specific surface area, pore structure, and scanning electron microscopy (SEM) images of the walnut shell biochar is available in Table S2 and Fig. S3 in the SI.

Effect of gas-solid fluidization. Gas-solid fluidization is a widely applied process for efficient gas-solid reaction by improving the heat and mass transfer rates. It also offers the possibility of continuous process coupled with high throughput. Plasma, especially plasmatron or plasma jet, can potentially combine with a fluidized bed for gas-solid or plasma catalytic reactions, whereas such a system has been rarely investigated for gas conversion processes [74-77]. It is therefore intriguing to explore the performance of a plasmatron fluidized bed for CO_2 conversion. To this end, in contrast to the fixed bed, the biochar in the experiments of this section was fluidized by the CO_2 plasmatron gas flow that contains a lot of active plasma species, forming a plasmatron fluidized bed system. A comparison of the CO_2 conversion and energy efficiency in the fixed bed and fluidized bed systems under different feed CO_2 flow rates is presented in Fig. 6, together with the photos of the two pattens.

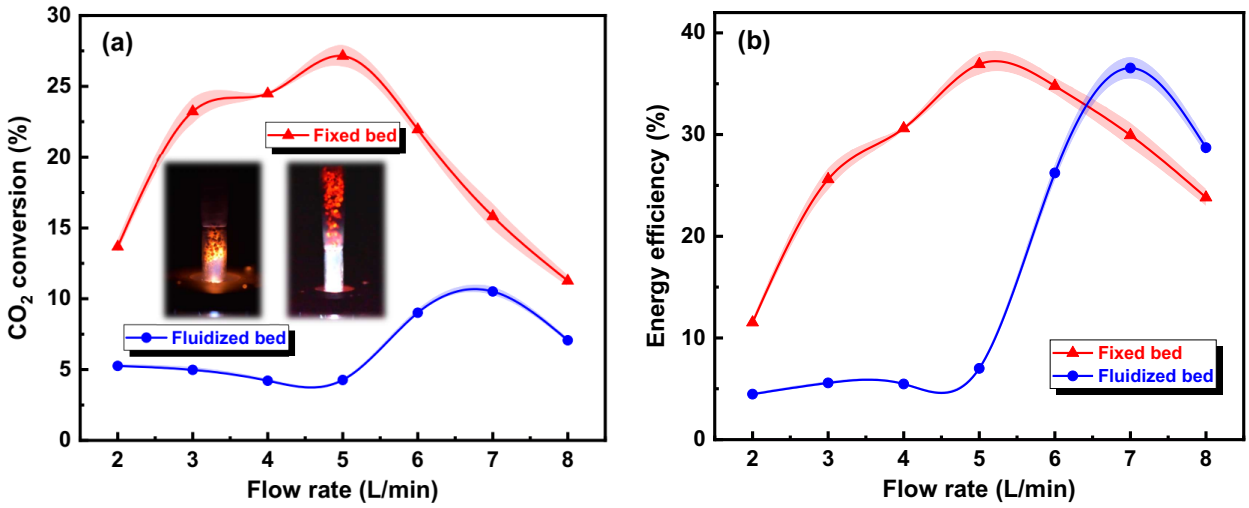

Fig. 6. CO_2 conversion (a) and energy efficiency (b) as a function of CO_2 flow rate in the plasmatron assisted CO_2 reaction with walnut shell biochar (pyrolyzed at 773K) in a fixed bed and fluidized bed. The photos of the fixed bed pattern and fluidized bed pattern are displayed in (a). Walnut shell biochar pyrolyzed at 773K was used.

A bit surprisingly, the fluidized bed pattern gives rise to a substantially lower CO_2 conversion in comparison to the fixed bed, although the energy efficiency of it at a higher feed flow rate (> 6 L/min) is slightly greater. The difference of the SEIs in the two cases is very limited with a small deviation (<17%) primarily at relatively high flow rates (see Fig. S1 in SI), and can therefore not account for the observed behavior. In order to further understand the difference in the reaction networks of the two cases, their online gas compositions at a typical CO_2 flow rate of 5 L/min as time elapses after plasma-on are studied and plotted in Fig. 7(a). Though the temporal conversion rate of solid carbon can provide additional insights into the reaction mechanisms, it is not directly measurable. So, the consumption rate of carbon (element) $C_C\,(\mathrm{mol/s})$ was first calculated, based on the carbon elemental balance before and after the reaction by reasonably assuming that the consumed carbon from biochar is converted merely

into CO and CO_2, as defined in Eq. (8). The temporal conversion of carbon $X_C(\%)$ was then obtained by dividing the integral of the consumption rate over time by the carbon content in the original biochar sample, as described in Eq. (9).

$$C_C\,(\mathrm{mol/s}) = \frac{Q_{out}\,(\mathrm{mol/min}) \times (100 - C_{(O_2\,out)}\,(\%)) - Q_{in}\,(\mathrm{mol/min})}{60} \tag{8}$$

$$X_C(\%) = \int \frac{C_C\,(\mathrm{mol/s}) \times 12\ \mathrm{g/mol}}{m_c \times \omega_{(C)}(\%)}\,\mathrm{d}t \tag{9}$$

where m_c is the mass of biochar, $\omega_{(C)}(\%)$ is the mass fraction of carbon from ultimate analysis.

The calculated consumption rate and conversion of carbon as time elapsed are plotted in Fig. 7(b) for both the fixed bed and fluidized bed cases. In addition, as the CO_2 decomposition pathway could kinetically contribute to the conversion of CO_2 as well in the plasma CO_2 reaction with biochar, its contribution was calculated, together with that of the CO_2 + C pathway, based on the oxygen-balance method described in Eqs. (5), (6). The results are plotted in Fig. 7(c).

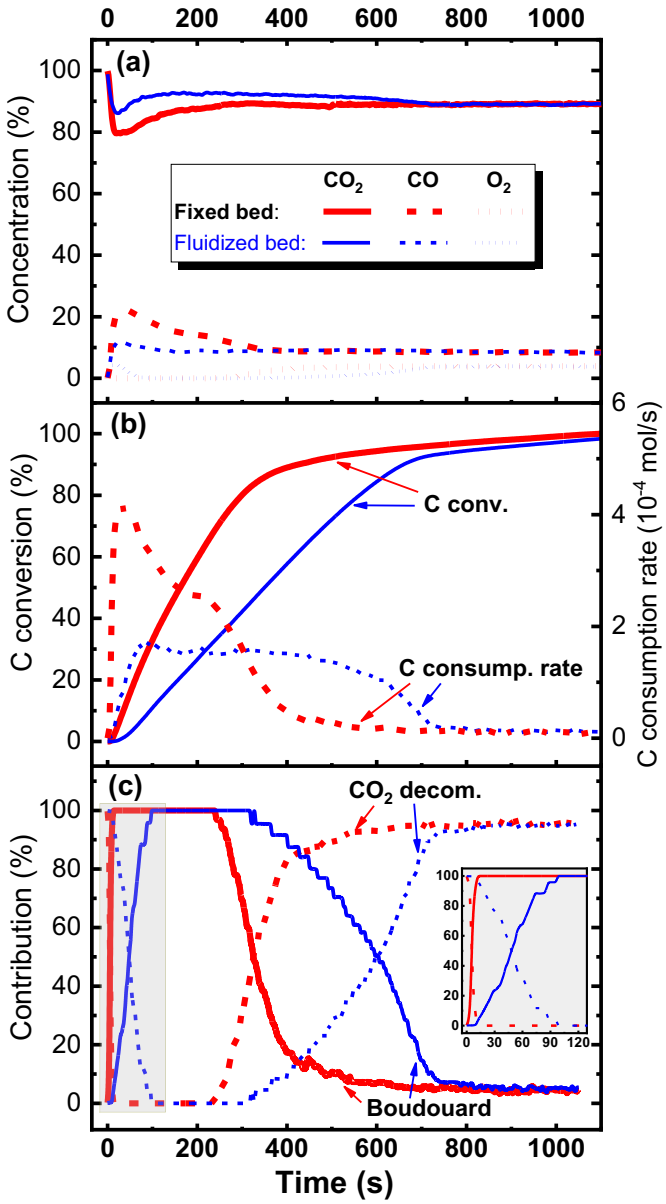

Fig. 7. Online concentrations of CO_2, CO, O_2 (a), calculated conversion and consumption rate of carbon element (b), as well as the contributions of CO_2 decomposition (CO_2 = CO + 1/2 O_2) and Boudouard reaction (CO_2 + C = 2CO) to the conversion of CO_2 (c) over time for the fixed bed pattern (thick lines in **red**) and fluidized bed pattern (thin lines in **blue**). The initial profiles after plasma-on in (c) are displayed in the inset for visualization. Feed CO_2 flow rate = 5 L/min; Walnut shell biochar pyrolyzed at 500 °C was used; m_c =1.2g; $\omega_{(C)}(\%)$=86.04% from Table 3.

As observed, the CO_2 conversion reaction occurred immediately after plasma on, yielding CO (and O_2), to different extents in the fixed and fluidized beds. In general, for a certain amount of biochar, the consumption rate of carbon and thus the rate of reaction between biochar and CO_2 plasma were higher in the fixed bed than those in the fluidized bed, as seen from the CO_2, CO concentrations, and the consumption rate and conversion of carbon showed in Fig. 7(a) and 7(b), respectively. A carbon conversion of 90% was achieved within ~420s after plasma-on in the fixed bed, whereas it took ~660s in the fluidized bed. Regarding the fixed bed system, the reaction rate reached a peak already at 20-30s with a maximum carbon consumption rate of ~0.42 mmol/s, as exhibited in Fig. 7(b). The carbon consumption rate rapidly decayed in a two-stage behavior to ~0.04 mmol/s at t =~ 420s (carbon conversion = ~90%), followed by a slow decrease to nearly 0 at t =~ 720s (carbon conversion = ~96%). The overall reaction rate in the fluidized bed system was shown to be significantly lower. The carbon consumption rate raised fast after plasma-on, but less rapidly than the fixed bed system. It reached the peak value of ~0.18 mmol/s only at t =~ 90s. The maximum obtained is only a half of that in the fixed bed system, but relatively stabilized for over 300s before it gradually decayed after t =~ 400s.

Contributions of the net CO_2 decomposition reaction ($CO_2 \rightarrow CO + 1/2O_2$) and Boudouard reaction ($CO_2 + C \rightarrow 2CO$) to the CO_2 conversion displayed in Fig. (7) can provide more insights on the reaction networks. In general, the overall Boudouard reaction was a dominant contributor in the overall conversion of CO_2, when the reactant biochar is still largely unreacted (see Fig. 7(b) as well). Nevertheless, it is interesting to note that the conversion of CO_2 after plasma-on is initiated by the net CO_2 decomposition reaction in both the fixed bed

and fluidized bed systems instead of the Boudouard reaction, as shown in the inset in Fig. 7(c). Consistently, an initial rise of the O_2 concentration is seen for both systems in Fig. 7(a). This behavior is associated with the two-stage configuration i.e., plasma generation and the biochar bed (see Fig. 1). The injected CO_2 experiences first the splitting reaction before reaching the biochar bed zone for the CO_2 + C reaction. As time elapses, the net reaction of CO_2 with biochar rapidly becomes the exclusive contributor, replacing the CO_2 decomposition route. The shift is done only within ~10s in the fixed bed case but would need up to ~100s for the fluidized bed. This is probably linked to the longer distance between the plasma generation zone and the biochar in the fluidized bed compared to the fixed bed, resulting insufficient contact between the CO_2 plasma and biochar, as seen from the photos in Fig. 6(a). As the biochar gets consumed, the CO_2 decomposition route starts playing an increasing role after t = ~240s in the fixed bed system but only after t = ~330s in the fluidized bed system. Comparing Fig. 7(b) and 7(c), it is interesting to note that the conversions of carbon at which the CO_2 decomposition becomes the dominant contributor to CO_2 conversion are both around 83% for the fixed bed and fluidized bed systems. In general, the profiles of the contribution of the Boudouard reaction (and CO_2 decomposition reaction) to CO_2 conversion (Fig. 7(c)) agree well with those of the carbon consumption rate profile (Fig. 7(b)) in terms of time-resolved variation. Also, as evidenced, the CO_2 decomposition process and Boudouard reaction could coexist at least for a certain time period in both the fixed bed and fluidized bed systems, *e.g.*, t = 250-650s and t = 300-750s, respectively (Fig. 7c). In the final state, when total consumption of carbon is nearly reached, both systems provide similar gas composition as a result of the CO_2 decomposition reaction.

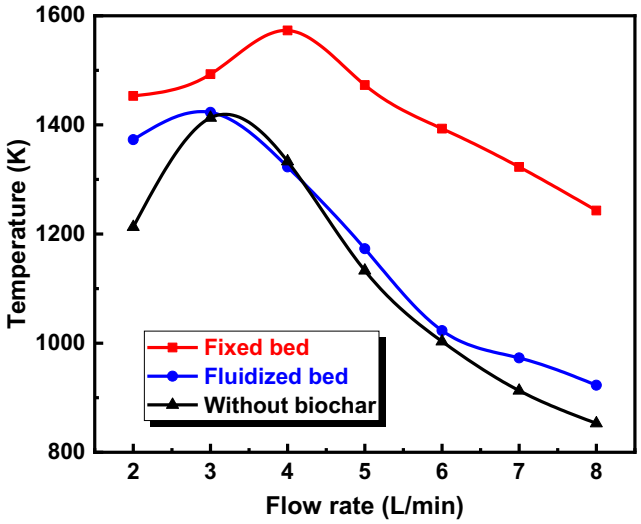

Fig. 8. Measured gas temperatures under the studied conditions by using the thermocouple placed 10 mm vertically above the screen mesh inside the quartz cover. Walnut shell biochar prepared at pyrolysis temperature of 773K was used.

Gas temperature in the gas-solid reaction region is a crucial factor influencing the reaction networks. Therefore it was measured for both the fixed bed and fluidized bed systems to understand the underlying kinetic reason for their observed difference in the reaction performance. The results under different flow rates for both systems together with the case in the absence of biochar (for comparison) are plotted in Fig. 8. Note that the thermocouple was placed apart from the plasma generation region and therefore, the given temperature here does not represent the plasma gas temperature upstream.

As can be noted, the gas temperature rises first upon increasing flow rate and then decreases for all the studied cases. A considerably higher temperature with a maximum of 1573K is reached (at flow rate = 4 L/min) in the fixed bed than that in the fluidized bed, where a peak of ~1423K is obtained (at flow rate = 3 L/min). This could to some extent contribute to a better CO_2 conversion performance in the fixed bed system, since the thermal chemistry is also

important in the plasmatron assisted CO_2 + C reaction, as discussed later in Section 3.4. Nevertheless, the gas temperature is conceivably not the most crucial factor resulting in the performance difference. For example, merely a temperature rise from 1423K in the fluidized bed to 1493K in the fixed bed at the same flow rate of 3 L/min can unlikely dramatically elevate the CO_2 conversion from ~5.0% to ~23.2%. More likely, in the fluidized bed, stronger reverse reactions between CO and O_2 (or O) proceed, giving rise to the regeneration of CO_2, due to the insufficient contact between the CO_2 plasma and biochar that reduces the probability of consuming O_2 (or O) by C. More discussions on the mechanisms will be given in the next section.

Electron energy distribution of the plasmatron and the role of plasma chemistry and thermochemistry. The CO_2 conversion routes in NTPs are strongly dependent on the fractions of electron energy transferred into different channels such as CO_2 excitation, ionization, and dissociation that could drive the activation of CO_2 differently [7]. Therefore, in order to elucidate the CO_2 conversion mechanisms, the determination of the electron density, electron temperature, vibrational temperature, and rotational temperature is of great significance. To this end, optical emission spectroscopy (OES), a powerful non-invasive diagnostic tool for plasma characterization, has been employed for the studied plasmatron CO_2 conversion processes. As above mentioned, only the spectra of the plasmatron CO_2 decomposition cases without biochar were collected. The electron density was calculated based on the Stark broadening of the O spectral line at 844.6 nm [78-81]. The electron temperature, vibrational temperature, and rotational temperature were derived by using the Boltzmann plot method

[82-84] based on selected Ar I, II lines, the Δv = 0 band of the CN Violet system at 385.5, 386.2, 387.1, 388.3 nm, and the C_2 (0, 0) Swan band centered at 516.5 nm, respectively, in the collected spectra under different flow rates. The calculation methods, the spectroscopic parameters for the selected spectral lines, as well as typical fitting of the profile and Boltzmann plots are available in Section S5 in SI. The obtained results are tabulated in Table 4. Note that for determining the electron density, a reasonably small amount of Ar (20%) was added into CO_2 to generate the needed Ar atomic spectral lines, following the previously reported method [85]. CN spectra were formed probably due to the presence of a trace amount of N_2 from the fed CO_2 gas or from the ambient air.

Moreover, the overall density of O atom, which is a key intermediate species in CO_2 conversion reactions, has been experimentally derived in this work based on the signal intensities of the Ar spectral line at 842 nm and O spectral line at 844.6 nm in the Ar-dopped CO_2 plasmatron, following the procedure reported in [86]. This is, to our knowledge, for the first time in an experimental study of NTP assisted CO_2 conversion. The results under different flow rates are given in Table 4 as well, providing valuable validation targets for further chemical kinetic modelling work. An O density of up to 10^{16} cm^{-3} is reached in the plasmatron CO_2 system, indicating the existence of strong CO_2 activation reactions.

Table 4 The electron density, and electron / vibrational / rotational temperature, O atom density of the CO_2 plasmatron under different flow rates

Flow rate	2 L/min	3 L/min	4 L/min	5 L/min	6 L/min	7 L/min	8 L/min
Electron density (10^{15} cm^{-3})	6.48±0.62	3.67±0.17	2.64±0.26	3.23±0.23	2.83±0.29	2.79±0.12	2.42±0.25
Electron temperature (eV)*	1.55±0.28	1.10±0.16	1.49±0.29	1.44±0.21	1.45±0.31	1.25±0.14	1.45±0.3
Vibrational temperature (K)	6340±808	7130±762	7240±641	6990±649	7000±640	7010±204	8170±846
Rotational temperature (K)	2370±110	2135±69	2348±123	2096±115	2189±92	2220±108	2125±119
O atom density (10^{16} cm^{-3})*	3.17±0.14	3.43±0.11	4.92±0.25	5.60±0.29	5.40±0.22	4.08±0.19	6.76±0.36

*The spectra of an 80%CO_2 + 20%Ar mixture were used for the determination.

An electron density of up to (2.43-6.48)·10^{15} cm^{-3} was achieved in the CO_2 plasmatron, as given in Table 4, which is several orders of magnitude higher than that in other typical NTPs such as DBD and corona (10^{9}-10^{13} cm^{-3}) [87-90]. This behavior allows for a high processing capacity, as

discussed in Section 3.1, and therefore industrially favorable. The electron energy in the CO_2 plasmatron is in the range of 1.1-1.5 eV for all the flow rates, which has been known as the most suitable for efficient vibrational excitation of CO_2 [7], corroborated by a relatively high vibrational temperature of 6300-8200K. Note that normally a remarkably lower vibrational temperature in other NTPs (*e.g.*, 3900-4500K [91, 92] for gliding arc, <3000K for DBD [93, 94]) is reported. This indicates the abundance of vibrational levels of CO_2 ($CO_2(v)$) that are driven by the electron-impact–vibrational-excitation *via* a so-called ladder-climbing way [7, 95]. The vibrationally stimulated route is known as the most effective channel for CO_2 dissociation in plasma [7, 24], which could partly explain the better performance obtained in the plasmatron than that of other typical NTPs for CO_2 decomposition, as discussed in Section 3.1. The dissociation of vibrationally excited states of CO_2 ($CO_2(v)$) *via* collision with O atoms (Eq. 10) is considered the dominant contributor to CO_2 conversion. In addition, the reaction of ground state CO_2 with O atoms (Eq. 11) as well as the electron-impact dissociation of $CO_2(v)$ (Eq. 12) could contribute to CO_2 conversion as well, but to a largely less extent. The electron-impact decomposition route of CO_2 that needs have enough energy of >7 eV [7, 95] is considered not important, due to the relatively low mean electron energy of the plasmatron (1.1-1.5 eV).

$$CO_2(v) + O \rightarrow CO + O_2 \quad (10)$$

$$CO_2(g) + O \rightarrow CO + O_2 \quad (11)$$

$$CO_2(v) + e \rightarrow CO + O + e \quad (12)$$

Rotational temperature can normally represent the gas temperature in atmospheric pressure plasmas because of the fast rational-translational relaxation [96]. As seen in Table 4, the plasmatron exhibits gas temperature of up to 2100-2400 K in the core arc plasma area,

featuring the property of a typical "warm plasma" [16, 40, 91, 97]. With such high gas temperatures, thermochemistry could already play a role in plasma chemical processes. Thermally driven CO_2 decomposition may proceed in the plasmatron, but its contribution could be very limited, since the conversion is only <8% at 2400K in a pure CO_2 system at thermodynamic equilibrium [26]. Also, such high temperatures could reach only in the very limited core area of the plasma arc and the residence time is therefore rather short (<25 ms). However, the thermodynamically more favorable recombination reactions between CO and O or O_2 can be largely stimulated under such high temperatures, generating CO_2 again [11, 24, 98]. In fact, the recombination reactions limit the CO_2 conversion in warm plasma assisted CO_2 dissociation process, as confirmed in previous experimental and modeling studies [11, 16, 23, 98]. On the other hand, the high-temperature plasma stream could result in a relatively high and desired gas temperature (<1573K, see Fig. 8) in the downstream gas-solid reaction zone and therefore favorably drive the biochar involved reactions by thermochemistry.

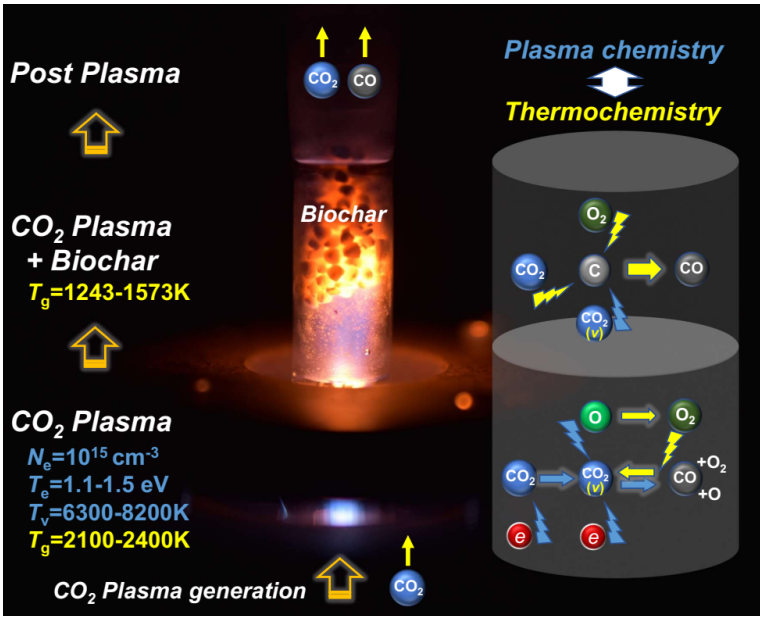

Fig. 9. Reaction scheme of the plasmatron assisted CO_2 reaction with biochar along the reactor. The fixed bed system is given as an example.

The reaction scheme is presented in Fig. 9 to illustrate clearly the potentially dominant mechanisms of the plasmatron assisted CO_2 reaction with biochar. The conversion of CO_2 experiences two stages along the reactor: the 1st CO_2 plasma stage and the 2nd stage in the presence of biochar. After plasma-on, before reaching the biochar region, CO_2 gets decomposed in the 1st stage, as already experimentally demonstrated in Section 3.2, primarily *via* the above discussed vibrationally stimulated routes in plasma chemistry. Nevertheless, the reverse reactions of CO_2 decomposition by thermochemistry are also of importance in this stage due to the abundance of CO, O_2 (or O) and the high gas temperature in the system. After CO_2 plasmatron reaches the biochar bed, the carbon-involved gas-solid reactions become dominant. The unreacted CO_2 can react directly with solid carbon through the Boudouard reaction (Eq. (1)), forming the desired CO. The generated O_2 (or O) from the 1st stage can then be consumed here due to their reactions with carbon, producing CO as well

with the presence of a sufficient amount of carbon. This explains why nearly no O_2 is detected in the plasmatron CO_2 reaction with biochar. This behavior is apparently industrially desirable due to the possible elimination of the subsequent costly purification processes. Continuous consumption of O_2 could then promote the forward reaction of CO_2 decomposition. Furthermore, in this stage, the thermochemistry is thought to be dominant since the gas temperature remains relatively high (*e.g.*, 1243-1573K in the fixed bed, see Fig. 8) and the oxidation of biochar is thermodynamically favorable. Also, the thermal reaction analysis showed that the reaction between CO_2 and C could theoretically give rise to CO_2 conversion already at temperatures of around 673K at 1 atm under thermodynamical equilibrium. As presented in Section 3.1, a conversion of <5.3% can be reached at 1273K in a tubular furnace under a similar residence time as that in the plasmatron. Plasma chemistry may proceed in the 2nd stage as well since the reactive CO_2 species formed in plasma with relatively long lifetimes (*e.g.*, $CO_2(v)$, a few μs [99]) can possibly react directly with biochar to produce CO [100], or collide with O atom to dissociate. Nevertheless, the role of plasma chemical reactions is presumably only to a very limited extent in this stage since the short-lived electrons probably mostly disappear in this region with the absence of an electric field. This could be partly confirmed from the observation in the OES study that no measurable spectra were collected for this stage by using the optical fiber. After passing through the gas-solid reaction zone in the 2nd stage, the gas stream carrying the formed CO and unreacted CO_2 does not undergo further reactions in the post plasma region due to the relatively low gas temperature. Further detailed modelling studies are necessary to quantitatively unravel the underlying kinetics.

It can be concluded that plasma chemistry and thermochemistry coexist in the plasmatron CO_2 reaction with biochar and their interaction enhances the overall performance of CO_2 conversion. The CO_2 dissociation is initiated in the 1st stage by primarily the vibrational-excitation-based plasma chemistry, whereas the thermochemistry dominates the 2nd stage for C + CO_2 and C + O_2 (O) reactions. The latter can to some extent promote the decomposition of CO_2 by continuously consuming the O_2 produced in the 1st stage. The 1st stage can not only provide a reactive plasma gas flow but also serve as a heat source for the 2nd stage to undergo thermal reactions.

Since the two stages designed in the plasmatron reactor are relatively far apart from each other, the produced O_2 in the 1st stage can largely recombine with CO to produce CO_2 *via* thermochemistry before reaching the 2nd stage to react with biochar, which however limits the conversion of CO_2 in this system. The experimental results can support this speculation that the fluidized bed system with a longer distance between the two stages exhibited considerably lower CO_2 conversion, as discussed in Section 3.3. In this regard, further improvement can be expected by combining the two stages together or moving them closer, in order to drive an instant consumption of the produced O_2 by biochar rather than by the desired product CO. Moreover, quenching the 1st stage selectively to inhibit the reverse reactions of CO_2 decomposition is also worthwhile, as already previously proposed [11]. Nevertheless, it should be kept in mind that the presence of solid biochar in plasma and quenching the plasma could affect the formation of a large plasma volume. Parameter studies are needed to find out the balance between the reaction performance and the plasma volume.

Summary and conclusions

The CO_2 reaction with biochar has been studied in this work in an atmospheric plasmatron, aiming for efficient CO_2 conversion into O_2-free CO. The reaction performance was evaluated under different conditions in terms of biochar type (walnut shell, sawdust, rice straw), pyrolysis temperature for biochar preparation (673, 773, 873K), and the gas-solid reaction pattern (fixed bed and fluidized bed). *In-situ* optical emission spectroscopy (OES) study has been performed to unravel the electron energy distribution of the plasma and elucidate the reaction mechanisms, with a focus on understanding the role of plasma chemistry and thermochemistry.

Results showed that the addition of biochar and the presence of the plasmatron both facilitated the conversion of CO_2 remarkably. A maximum CO_2 conversion of 27.1% can be achieved in the plasmatron assisted CO_2 reaction with biochar, while no conversion was observed in the thermal CO_2 decomposition experiments under the studied conditions. Also importantly, nearly no O_2 was produced in this process. A comparison of the results with those reported in the literature for CO_2 splitting in non-thermal plasmas showed that the immediate system is among the best in the overall performance in terms of CO_2 conversion (max. 27.1%), energy efficiency (max. 36.9%), and processing capacity (2-8 L/min).

Biochar properties affected the CO_2 conversion performance considerably and the carbon content plays a decisive role. Walnut shell biochar prepared at relatively high pyrolysis temperatures of 773K and 873K exhibited the best CO_2 conversion and energy efficiency. The pattern of gas-solid reaction was shown to be of importance as well to the reaction

performance. A fixed bed system showed significantly better results in comparison to a fluidized bed system, probably owing to a prompt consumption of O_2 by biochar that retarded the recombination reactions of CO_2. In both systems, the conversion of CO_2 was proved to be initiated by the CO_2 dissociation reactions rather than the reactions with biochar.

The OES derived results showed that the plasmatron features a notably higher electron density of up to 10^{15} cm^{-3} in comparison to typical non-thermal plasmas such as dielectric barrier discharge and corona discharge (10^{9}-10^{13} cm^{-3}), enabling a high processing capacity. The moderate electron temperature (1.1-1.5 eV) facilitates an efficient vibrational excitation of CO_2, as evidenced by the high vibrational temperature (6300-8200K). This behavior facilitates the most effective channel for CO_2 dissociation in plasmas. A relatively high rotational (gas) temperature is reached in the core plasma area (2100-2400K), indicating the possible importance of thermochemistry in the plasmatron chemical process. A two-stage reaction network proceeds in the plasmatron assisted CO_2 reaction with biochar, where plasma chemistry dominates in the 1st stage for CO_2 dissociation while thermochemistry dominates in the 2nd stage for the reactions of CO_2 + C and O_2 + C to produce CO. Continuous consumption of the produced O_2 by biochar from the 1st stage can promote the forward reactions of CO_2 dissociation. Consequently, the co-existence and interaction of plasma chemistry and thermochemistry allow for an efficient conversion of CO_2 into CO in the presence of biochar.

The investigated plasmatron assisted CO_2 reaction with biochar showed promise for effective conversion of CO_2 into O_2-free fuel gas CO. Nevertheless, further improvement of the reaction performance can still be expected by inhibiting the thermally stimulated reverse reactions of CO_2 dissociation.

Associated Content

Supporting Information is available:

Supporting Information (SI): Further information on (1) the determination of the outlet gas flow rate, (2) the specific energy input, (3) the results of thermal CO_2 + C experiments, (4) the specific surface area, pore structure, and scanning electron microscopy (SEM) images of the walnut shell biochar as well as (5) the determination of electron density, electron / vibrational / rotational temperatures, and O atom density.

Acknowledgement

This work was supported by the National Key Technologies R&D Program of China (No. 2018YFE0117300), and the National Natural Science Foundation of China (No. 52076190 and No. 51976191). C. Wu and X. Tu acknowledge the funding from the European Union's Horizon 2020 research and innovation programme under the Marie Sklodowska-Curie grant agreement No. 823745.

Credit author statement

HZ: Conceptualization, Investigation, Formal Analysis, Writing - Original draft preparation

QT: Investigation, Formal Analysis, Writing - Original draft preparation

QH: Conceptualization, Supervision, Project administration, Writing-Review and editing

KW: Investigation

XT: Validation, Writing-Review and editing

XZ: Validation, Writing-Review and editing

CW: Validation, Writing-Review and editing

JY: Supervision, Writing-Review and editing

XL: Conceptualization, Supervision, Project administration, Writing-Review and editing

Authors Information

Corresponding Authors

Hao Zhang - *State Key Laboratory of Clean Energy Utilization, Zhejiang University, Hangzhou 310027, People's Republic of China*

Xin Tu - *Department of Electrical Engineering and Electronics, University of Liverpool, Liverpool L69 3GJ, U.K.*

Authors

Qinhuai Tan - *State Key Laboratory of Clean Energy Utilization, Zhejiang University, Hangzhou 310027, People's Republic of China*

Qunxing Huang - *State Key Laboratory of Clean Energy Utilization, Zhejiang University, Hangzhou 310027, People's Republic of China*

Kaiyi Wang - *State Key Laboratory of Clean Energy Utilization, Zhejiang University, Hangzhou 310027, People's Republic of China*

Xiaotong Zhao - *State Key Laboratory of Clean Energy Utilization, Zhejiang University, Hangzhou 310027, People's Republic of China; School of Chemistry and Chemical Engineering, Queen's University Belfast, Belfast BT7 1NN, UK*

Chunfei Wu - *School of Chemistry and Chemical Engineering, Queen's University Belfast, Belfast BT7 1NN, UK*

Jianhua Yan - *State Key Laboratory of Clean Energy Utilization, Zhejiang University, Hangzhou 310027, People's Republic of China*

Xiaodong Li - *State Key Laboratory of Clean Energy Utilization, Zhejiang University, Hangzhou 310027, People's Republic of China*

Reference

[1] S. Dang, B. Qin, Y. Yang, H. Wang, J. Cai, Y. Han, S. Li, P. Gao, Y. Sun, Rationally designed indium oxide catalysts for CO₂ hydrogenation to methanol with high activity and selectivity, Science Advances 6(25) (2020) eaaz2060. https://doi.org/doi:10.1126/sciadv.aaz2060.

[2] M. Liu, Y. Pang, B. Zhang, P. De Luna, O. Voznyy, J. Xu, X. Zheng, C.T. Dinh, F. Fan, C. Cao, F.P.G. de Arquer, T.S. Safaei, A. Mepham, A. Klinkova, E. Kumacheva, T. Filleter, D. Sinton, S.O. Kelley, E.H. Sargent, Enhanced electrocatalytic CO2 reduction via field-induced reagent concentration, Nature 537(7620) (2016) 382-386. https://doi.org/10.1038/nature19060.

[3] J. Artz, T.E. Müller, K. Thenert, J. Kleinekorte, R. Meys, A. Sternberg, A. Bardow, W. Leitner, Sustainable Conversion of Carbon Dioxide: An Integrated Review of Catalysis and Life Cycle Assessment, Chemical Reviews 118(2) (2018) 434-504. https://doi.org/10.1021/acs.chemrev.7b00435.

[4] H. Xu, J. Ma, P. Tan, Z. Wu, Y. Zhang, M. Ni, J. Xuan, Enabling thermal-neutral electrolysis for CO2-to-fuel conversions with a hybrid deep learning strategy, Energy Conversion and Management 230 (2021) 113827. https://doi.org/https://doi.org/10.1016/j.enconman.2021.113827.

[5] S.-Y. Pan, P.-C. Chiang, W. Pan, H. Kim, Advances in state-of-art valorization technologies for captured CO2 toward sustainable carbon cycle, Critical Reviews in Environmental Science and Technology 48(5) (2018) 471-534. https://doi.org/10.1080/10643389.2018.1469943.

[6] S. Rayne, Thermal Carbon Dioxide Splitting: A Summary of the Peer-Reviewed Scientific Literature, Nature Precedings (2008). https://doi.org/10.1038/npre.2008.1741.2.

[7] R. Snoeckx, A. Bogaerts, Plasma technology – a novel solution for CO2 conversion?, Chemical Society Reviews 46(19) (2017) 5805-5863. https://doi.org/10.1039/C6CS00066E.
[8] A. Galadima, O. Muraza, Catalytic thermal conversion of CO2 into fuels: Perspective and challenges, Renewable and Sustainable Energy Reviews 115 (2019) 109333. https://doi.org/https://doi.org/10.1016/j.rser.2019.109333.
[9] A. George, B. Shen, M. Craven, Y. Wang, D. Kang, C. Wu, X. Tu, A Review of Non-Thermal Plasma Technology: A novel solution for CO2 conversion and utilization, Renewable and Sustainable Energy Reviews 135 (2021) 109702. https://doi.org/https://doi.org/10.1016/j.rser.2020.109702.
[10] A. Bogaerts, X. Tu, J.C. Whitehead, G. Centi, L. Lefferts, O. Guaitella, F. Azzolina-Jury, H.-H. Kim, A.B. Murphy, W.F. Schneider, T. Nozaki, J.C. Hicks, A. Rousseau, F. Thevenet, A. Khacef, M. Carreon, The 2020 plasma catalysis roadmap, Journal of Physics D: Applied Physics 53(44) (2020) 443001. https://doi.org/10.1088/1361-6463/ab9048.
[11] A. Bogaerts, G. Centi, Plasma Technology for CO2 Conversion: A Personal Perspective on Prospects and Gaps, Frontiers in Energy Research 8 (2020) 111. https://doi.org/10.3389/fenrg.2020.00111.
[12] G. Chen, R. Snyders, N. Britun, CO2 conversion using catalyst-free and catalyst-assisted plasma-processes: Recent progress and understanding, Journal of CO2 Utilization 49 (2021) 101557. https://doi.org/https://doi.org/10.1016/j.jcou.2021.101557.
[13] H. Zhang, R. Xu, A. J, J. Zheng, J. Wan, K. Wang, B. Lan, J. Yan, X. Li, Destruction of biomass tar model compound in a rotating gliding arc plasma catalytic system: Contribution of typical transition metals in Ni-based bimetallic catalyst, Fuel 323 (2022) 124385. https://doi.org/https://doi.org/10.1016/j.fuel.2022.124385.
[14] H. Zhang, F. Zhu, X. Li, R. Xu, L. Li, J. Yan, X. Tu, Steam reforming of toluene and naphthalene as tar surrogate in a gliding arc discharge reactor, Journal of Hazardous Materials 369 (2019) 244-253. https://doi.org/https://doi.org/10.1016/j.jhazmat.2019.01.085.
[15] G. Chen, X. Tu, G. Homm, A. Weidenkaff, Plasma pyrolysis for a sustainable hydrogen economy, Nature Reviews Materials 7(5) (2022) 333-334. https://doi.org/10.1038/s41578-022-00439-8.
[16] H. Zhang, L. Li, X. Li, W. Wang, J. Yan, X. Tu, Warm plasma activation of CO2 in a rotating gliding arc discharge reactor, Journal of CO2 Utilization 27 (2018) 472-479. https://doi.org/https://doi.org/10.1016/j.jcou.2018.08.020.
[17] L. Li, H. Zhang, X. Li, J. Huang, X. Kong, R. Xu, X. Tu, Magnetically enhanced gliding arc discharge for CO2 activation, Journal of CO2 Utilization 35 (2020) 28-37. https://doi.org/https://doi.org/10.1016/j.jcou.2019.08.021.
[18] L. Wang, Y. Yi, H. Guo, X. Tu, Atmospheric Pressure and Room Temperature Synthesis of Methanol through Plasma-Catalytic Hydrogenation of CO2, ACS Catalysis 8(1) (2018) 90-100. https://doi.org/10.1021/acscatal.7b02733.
[19] L. Wang, Y. Yi, C. Wu, H. Guo, X. Tu, One-Step Reforming of CO2 and CH4 into High-Value Liquid Chemicals and Fuels at Room Temperature by Plasma-Driven Catalysis, Angewandte Chemie International Edition 56(44) (2017) 13679-13683. https://doi.org/https://doi.org/10.1002/anie.201707131.
[20] J. Huang, H. Zhang, Q. Tan, L. Li, R. Xu, Z. Xu, X. Li, Enhanced conversion of CO2 into O2-free fuel gas via the Boudouard reaction with biochar in an atmospheric plasmatron, Journal of CO2 Utilization 45 (2021) 101429. https://doi.org/https://doi.org/10.1016/j.jcou.2020.101429.
[21] H. Zhang, L. Li, R. Xu, J. Huang, N. Wang, X. Li, X. Tu, Plasma-enhanced catalytic activation of CO2 in a modified gliding arc reactor, Waste Disposal & Sustainable Energy 2(2) (2020) 139-150. https://doi.org/10.1007/s42768-020-00034-z.
[22] J.-L. Liu, H.-W. Park, W.-J. Chung, D.-W. Park, High-Efficient Conversion of CO2 in AC-Pulsed Tornado Gliding Arc Plasma, Plasma Chemistry and Plasma Processing 36(2) (2016) 437-449. https://doi.org/10.1007/s11090-015-9649-2.
[23] L. Li, H. Zhang, X. Li, X. Kong, R. Xu, K. Tay, X. Tu, Plasma-assisted CO2 conversion in a gliding arc discharge: Improving performance by optimizing the reactor design, Journal of CO2 Utilization 29 (2019) 296-303. https://doi.org/https://doi.org/10.1016/j.jcou.2018.12.019.

[24] W. Wang, D. Mei, X. Tu, A. Bogaerts, Gliding arc plasma for CO2 conversion: Better insights by a combined experimental and modelling approach, Chemical Engineering Journal 330 (2017) 11-25. https://doi.org/https://doi.org/10.1016/j.cej.2017.07.133.
[25] Y. Uytdenhouwen, K.M. Bal, I. Michielsen, E.C. Neyts, V. Meynen, P. Cool, A. Bogaerts, How process parameters and packing materials tune chemical equilibrium and kinetics in plasma-based CO2 conversion, Chemical Engineering Journal 372 (2019) 1253-1264. https://doi.org/https://doi.org/10.1016/j.cej.2019.05.008.
[26] D. Mei, X. Tu, Conversion of CO2 in a cylindrical dielectric barrier discharge reactor: Effects of plasma processing parameters and reactor design, Journal of CO2 Utilization 19 (2017) 68-78. https://doi.org/https://doi.org/10.1016/j.jcou.2017.02.015.
[27] F. Zhu, H. Zhang, X. Yan, J. Yan, M. Ni, X. Li, X. Tu, Plasma-catalytic reforming of CO2-rich biogas over Ni/γ-Al2O3 catalysts in a rotating gliding arc reactor, Fuel 199 (2017) 430-437. https://doi.org/https://doi.org/10.1016/j.fuel.2017.02.082.
[28] F. Ahmad, E. Lovell, H. Masood, P.J. Cullen, K. Ostrikov, J. Scott, R. Amal, Low-Temperature CO 2 Methanation: Synergistic Effects in Plasma-Ni Hybrid Catalytic System, ACS Sustainable Chemistry & Engineering XXXX (2020). https://doi.org/10.1021/acssuschemeng.9b06180.
[29] S. Kelly, J.A. Sullivan, CO2 Decomposition in CO2 and CO2/H2 Spark-like Plasma Discharges at Atmospheric Pressure, ChemSusChem 12(16) (2019) 3785-3791. https://doi.org/https://doi.org/10.1002/cssc.201901744.
[30] R. Aerts, R. Snoeckx, A. Bogaerts, In-Situ Chemical Trapping of Oxygen in the Splitting of Carbon Dioxide by Plasma, Plasma Processes and Polymers 11(10) (2014) 985-992. https://doi.org/https://doi.org/10.1002/ppap.201400091.
[31] P. Lahijani, Z.A. Zainal, M. Mohammadi, A.R. Mohamed, Conversion of the greenhouse gas CO2 to the fuel gas CO via the Boudouard reaction: A review, Renewable and Sustainable Energy Reviews 41 (2015) 615-632. https://doi.org/https://doi.org/10.1016/j.rser.2014.08.034.
[32] D. Woolf, J.E. Amonette, F.A. Street-Perrott, J. Lehmann, S. Joseph, Sustainable biochar to mitigate global climate change, Nature Communications 1(1) (2010) 56. https://doi.org/10.1038/ncomms1053.
[33] J. Wang, S. Wang, Preparation, modification and environmental application of biochar: A review, Journal of Cleaner Production 227 (2019) 1002-1022. https://doi.org/https://doi.org/10.1016/j.jclepro.2019.04.282.
[34] R.-s. Xu, J.-l. Zhang, G.-w. Wang, H.-b. Zuo, P.-c. Zhang, J.-g. Shao, Gasification behaviors and kinetic study on biomass chars in CO2 condition, Chemical Engineering Research and Design 107 (2016) 34-42. https://doi.org/https://doi.org/10.1016/j.cherd.2015.10.014.
[35] Y. Liu, L. Liu, L. Hong, Gasification of char with CO2 to produce CO – Impact of catalyst carbon interface, Catalysis Today 281 (2017) 352-359. https://doi.org/https://doi.org/10.1016/j.cattod.2016.04.006.
[36] G. Wang, J. Zhang, X. Hou, J. Shao, W. Geng, Study on CO2 gasification properties and kinetics of biomass chars and anthracite char, Bioresource Technology 177 (2015) 66-73. https://doi.org/https://doi.org/10.1016/j.biortech.2014.11.063.
[37] H.-H. Bui, L. Wang, K.-Q. Tran, Ø. Skreiberg, CO2 gasification of charcoals produced at various pressures, Fuel Processing Technology 152 (2016) 207-214. https://doi.org/https://doi.org/10.1016/j.fuproc.2016.06.033.
[38] Y.T. Kim, D.K. Seo, J. Hwang, Study of the Effect of Coal Type and Particle Size on Char–CO2 Gasification via Gas Analysis, Energy & Fuels 25(11) (2011) 5044-5054. https://doi.org/10.1021/ef200745x.
[39] F. Min, M. Zhang, Y. Zhang, Y. Cao, W.-P. Pan, An experimental investigation into the gasification reactivity and structure of agricultural waste chars, Journal of Analytical and Applied Pyrolysis 92(1) (2011) 250-257. https://doi.org/https://doi.org/10.1016/j.jaap.2011.06.005.
[40] H. Zhang, W. Wang, X. Li, L. Han, M. Yan, Y. Zhong, X. Tu, Plasma activation of methane for hydrogen production in a N2 rotating gliding arc warm plasma: A chemical kinetics study, Chemical Engineering Journal 345 (2018) 67-78. https://doi.org/https://doi.org/10.1016/j.cej.2018.03.123.

[41] R. Liu, R. Tsiava, S. Xu, D. Chen, Experimental study of char gasification characteristics with high temperature flue gas, Journal of the Energy Institute 97 (2021) 187-193. https://doi.org/https://doi.org/10.1016/j.joei.2021.04.015.
[42] D. Chen, Z. Zheng, K. Fu, Z. Zeng, J. Wang, M. Lu, Torrefaction of biomass stalk and its effect on the yield and quality of pyrolysis products, Fuel 159 (2015) 27-32. https://doi.org/https://doi.org/10.1016/j.fuel.2015.06.078.
[43] Y. Zhang, J. Zhang, F. Chen, H. Ma, D. Chen, Influence of biochar with loaded metal salts on the cracking of pyrolysis volatiles from corn straw, Energy Sources, Part A: Recovery, Utilization, and Environmental Effects (2020) 1-10. https://doi.org/10.1080/15567036.2020.1779414.
[44] R. Snoeckx, S. Heijkers, K. Van Wesenbeeck, S. Lenaerts, A. Bogaerts, CO2 conversion in a dielectric barrier discharge plasma: N2 in the mix as a helping hand or problematic impurity?, Energy & Environmental Science 9(3) (2016) 999-1011. https://doi.org/10.1039/C5EE03304G.
[45] S.R. Sun, H.X. Wang, D.H. Mei, X. Tu, A. Bogaerts, CO 2 conversion in a gliding arc plasma: Performance improvement based on chemical reaction modeling, J. CO2 Util. 17 (2017) 220-234. https://doi.org/10.1016/j.jcou.2016.12.009.
[46] D. Nagassou, S. Mohsenian, M. Nallar, P. Yu, H.-W. Wong, J.P. Trelles, Decomposition of CO2 in a solar-gliding arc plasma reactor: Effects of water, nitrogen, methane, and process optimization, Journal of CO2 Utilization 38 (2020) 39-48. https://doi.org/10.1016/j.jcou.2020.01.007.
[47] T. Nunnally, K. Gutsol, A. Rabinovich, A. Fridman, A. Gutsol, A. Kemoun, Dissociation of CO2in a low current gliding arc plasmatron, Journal of Physics D: Applied Physics 44(27) (2011). https://doi.org/10.1088/0022-3727/44/27/274009.
[48] M. Ramakers, G. Trenchev, S. Heijkers, W. Wang, A. Bogaerts, Gliding Arc Plasmatron: Providing an Alternative Method for Carbon Dioxide Conversion, ChemSusChem 10(12) (2017) 2642-2652. https://doi.org/10.1002/cssc.201700589.
[49] L.F. Spencer, A.D. Gallimore, CO2dissociation in an atmospheric pressure plasma/catalyst system: a study of efficiency, Plasma Sources Science and Technology 22(1) (2012). https://doi.org/10.1088/0963-0252/22/1/015019.
[50] D. Mansfeld, S. Sintsov, N. Chekmarev, A. Vodopyanov, Conversion of carbon dioxide in microwave plasma torch sustained by gyrotron radiation at frequency of 24 GHz at atmospheric pressure, Journal of CO2 Utilization 40 (2020). https://doi.org/10.1016/j.jcou.2020.101197.
[51] Y. Qin, G. Niu, X. Wang, D. Luo, Y. Duan, Conversion of CO2 in a low-powered atmospheric microwave plasma: In-depth study on the trade-off between CO2 conversion and energy efficiency, Chemical Physics 538 (2020). https://doi.org/10.1016/j.chemphys.2020.110913.
[52] G. Chen, N. Britun, T. Godfroid, V. Georgieva, R. Snyders, M.-P. Delplancke-Ogletree, An overview of CO2conversion in a microwave discharge: the role of plasma-catalysis, Journal of Physics D: Applied Physics 50(8) (2017). https://doi.org/10.1088/1361-6463/aa5616.
[53] W. Bongers, H. Bouwmeester, B. Wolf, F. Peeters, S. Welzel, D. van den Bekerom, N. den Harder, A. Goede, M. Graswinckel, P.W. Groen, J. Kopecki, M. Leins, G. van Rooij, A. Schulz, M. Walker, R. van de Sanden, Plasma-driven dissociation of CO2
for fuel synthesis, Plasma Processes and Polymers 14(6) (2017). https://doi.org/10.1002/ppap.201600126.
[54] G.J. van Rooij, D.C. van den Bekerom, N. den Harder, T. Minea, G. Berden, W.A. Bongers, R. Engeln, M.F. Graswinckel, E. Zoethout, M.C. van de Sanden, Taming microwave plasma to beat thermodynamics in CO2 dissociation, Faraday Discussions 183 (2015) 233-48. https://doi.org/10.1039/c5fd00045a.
[55] R. Aerts, W. Somers, A. Bogaerts, Carbon dioxide splitting in a dielectric barrier discharge plasma: a combined experimental and computational study, ChemSusChem 8(4) (2015) 702-16. https://doi.org/10.1002/cssc.201402818.

[56] Q. Yu, M. Kong, T. Liu, J. Fei, X. Zheng, Characteristics of the Decomposition of CO2 in a Dielectric Packed-Bed Plasma Reactor, Plasma Chemistry and Plasma Processing 32(1) (2011) 153-163. https://doi.org/10.1007/s11090-011-9335-y.
[57] I. Michielsen, Y. Uytdenhouwen, J. Pype, B. Michielsen, J. Mertens, F. Reniers, V. Meynen, A. Bogaerts, CO2 dissociation in a packed bed DBD reactor: First steps towards a better understanding of plasma catalysis, Chemical Engineering Journal 326 (2017) 477-488. https://doi.org/10.1016/j.cej.2017.05.177.
[58] K. Van Laer, A. Bogaerts, Improving the Conversion and Energy Efficiency of Carbon Dioxide Splitting in a Zirconia-Packed Dielectric Barrier Discharge Reactor, Energy Technology 3(10) (2015) 1038-1044. https://doi.org/10.1002/ente.201500127.
[59] B. Wang, X. Wang, H. Su, Influence of Electrode Interval and Barrier Thickness in the Segmented Electrode Micro-plasma DBD Reactor on CO2 Decomposition, Plasma Chemistry and Plasma Processing 40(5) (2020) 1189-1206. https://doi.org/10.1007/s11090-020-10091-1.
[60] Y. Uytdenhouwen, S. Van Alphen, I. Michielsen, V. Meynen, P. Cool, A. Bogaerts, A packed-bed DBD micro plasma reactor for CO2 dissociation: Does size matter?, Chemical Engineering Journal 348 (2018) 557-568. https://doi.org/10.1016/j.cej.2018.04.210.
[61] D. Mei, X. Zhu, Y.-L. He, J.D. Yan, X. Tu, Plasma-assisted conversion of CO2in a dielectric barrier discharge reactor: understanding the effect of packing materials, Plasma Sources Science and Technology 24(1) (2014). https://doi.org/10.1088/0963-0252/24/1/015011.
[62] Q. Huang, D. Zhang, D. Wang, K. Liu, A.W. Kleyn, Carbon dioxide dissociation in non-thermal radiofrequency and microwave plasma, Journal of Physics D: Applied Physics 50(29) (2017). https://doi.org/10.1088/1361-6463/aa754e.
[63] L.F. Spencer, A.D. Gallimore, Efficiency of CO2 Dissociation in a Radio-Frequency Discharge, Plasma Chemistry and Plasma Processing 31(1) (2010) 79-89. https://doi.org/10.1007/s11090-010-9273-0.
[64] W. Xu, M.-W. Li, G.-H. Xu, Y.-L. Tian, Decomposition of CO2Using DC Corona Discharge at Atmospheric Pressure, Japanese Journal of Applied Physics 43(12) (2004) 8310-8311. https://doi.org/10.1143/jjap.43.8310.
[65] M.S. Bak, S.-K. Im, M. Cappelli, Nanosecond-pulsed discharge plasma splitting of carbon dioxide, IEEE Transactions on Plasma Science 43(4) (2015) 1002-1007. https://doi.org/10.1109/tps.2015.2408344.
[66] Y. Wen, X. Jiang, Decomposition of CO2 Using Pulsed Corona Discharges Combined with Catalyst, Plasma Chemistry and Plasma Processing 21(4) (2001) 665-678. https://doi.org/10.1023/A:1012011420757.
[67] S.L. Brock, M. Marquez, S.L. Suib, Y. Hayashi, H. Matsumoto, Plasma Decomposition of CO2in the Presence of Metal Catalysts, Journal of Catalysis 180(2) (1998) 225-233. https://doi.org/https://doi.org/10.1006/jcat.1998.2258.
[68] G.-s. Liu, A.G. Tate, G.W. Bryant, T.F. Wall, Mathematical modeling of coal char reactivity with CO2 at high pressures and temperatures, Fuel 79(10) (2000) 1145-1154. https://doi.org/https://doi.org/10.1016/S0016-2361(99)00274-4.
[69] L. Zhang, J. Huang, Y. Fang, Y. Wang, Gasification Reactivity and Kinetics of Typical Chinese Anthracite Chars with Steam and CO2, Energy & Fuels 20(3) (2006) 1201-1210. https://doi.org/10.1021/ef050343o.
[70] J. Fermoso, C. Stevanov, B. Moghtaderi, B. Arias, C. Pevida, M.G. Plaza, F. Rubiera, J.J. Pis, High-pressure gasification reactivity of biomass chars produced at different temperatures, Journal of Analytical and Applied Pyrolysis 85(1) (2009) 287-293. https://doi.org/https://doi.org/10.1016/j.jaap.2008.09.017.
[71] S. Yuan, X.-l. Chen, J. Li, F.-c. Wang, CO2 Gasification Kinetics of Biomass Char Derived from High-Temperature Rapid Pyrolysis, Energy & Fuels 25(5) (2011) 2314-2321. https://doi.org/10.1021/ef200051z.
[72] S. Ergun, Kinetics of the Reaction of Carbon with Carbon Dioxide, Journal of Physical Chemistry 60(4) (1956) 480-485. https://doi.org/10.1021/j150538a022.

[73] X.-X. Xu, Synthesis and Characterization of Novel Chiral Liquid Crystalline Monomers and Polymers Derived From Menthol, Molecular Crystals and Liquid Crystals 557(1) (2012) 118-125. https://doi.org/10.1080/15421406.2011.637390.
[74] P. Jiang, A. Mahmud Parvez, Y. Meng, X. Dong, M. Xu, X. Luo, K. Shi, T. Wu, Novel two-stage fluidized bed-plasma gasification integrated with SOFC and chemical looping combustion for the high efficiency power generation from MSW: A thermodynamic investigation, Energy Conversion and Management 236 (2021) 114066. https://doi.org/https://doi.org/10.1016/j.enconman.2021.114066.
[75] K.J.M. del Campo Rodriguez, Valorization of Carbon Dioxide for the Production of Value-Added Chemicals in Fluidized Bed and Plasma-Catalytic Reactors, McGill University (Canada), 2021.
[76] N. Bouchoul, H. Touati, E. Fourré, J.-M. Clacens, C. Batiot-Dupeyrat, Efficient plasma-catalysis coupling for CH4 and CO2 transformation in a fluidized bed reactor: Comparison with a fixed bed reactor, Fuel 288 (2021) 119575. https://doi.org/https://doi.org/10.1016/j.fuel.2020.119575.
[77] Q. Wang, Y. Cheng, Y. Jin, Dry reforming of methane in an atmospheric pressure plasma fluidized bed with Ni/γ-Al2O3 catalyst, Catalysis Today 148(3) (2009) 275-282. https://doi.org/https://doi.org/10.1016/j.cattod.2009.08.008.
[78] J. Cen, Q. Hou, P. Yuan, J. Zhang, M. Sun, J. Pan, Z. Cao, Electron density measurement of a lightning stepped leader by oxygen spectral lines, AIP Advances 8(8) (2018). https://doi.org/10.1063/1.5042509.
[79] A.M. El Sherbini, A.M. Aboulfotouh, C.G. Parigger, Electron number density measurements using laser-induced breakdown spectroscopy of ionized nitrogen spectral lines, Spectrochimica Acta Part B: Atomic Spectroscopy 125 (2016) 152-158. https://doi.org/10.1016/j.sab.2016.10.003.
[80] H. Hegazy, Oxygen spectral lines for diagnostics of atmospheric laser-induced plasmas, Applied Physics B-Lasers and Optics 98(2-3) (2009) 601-606. https://doi.org/10.1007/s00340-009-3670-1.
[81] J. Plavčan, Determination of Stark Broadening Parameters for O, N from Hα Using Laser Induced Breakdown Spectroscopy, 2010, p. 101.
[82] X. Tu, H.J. Gallon, J.C. Whitehead, Electrical and spectroscopic diagnostics of a single-stage plasma-catalysis system: effect of packing with TiO2, Journal of Physics D: Applied Physics 44(48) (2011). https://doi.org/10.1088/0022-3727/44/48/482003.
[83] B. Ogungbesan, R. Kumar, L. Su, M. Sassi, Experimental validation of local thermal equilibrium in a MW plasma torch for hydrogen production, International Journal of Hydrogen Energy 38(35) (2013) 15210-15218. https://doi.org/10.1016/j.ijhydene.2013.09.099.
[84] Z. Gavare, A. Svagere, M. Zinge, G. Revalde, V. Fyodorov, Determination of gas temperature of high-frequency low-temperature electrodeless plasma using molecular spectra of hydrogen and hydroxyl-radical, Journal of Quantitative Spectroscopy and Radiative Transfer 113(13) (2012) 1676-1682. https://doi.org/10.1016/j.jqsrt.2012.04.022.
[85] R. Gessman, C. Laux, C. Kruger, Experimental study of kinetic mechanisms of recombining atmospheric pressure air plasmas, 1997. https://doi.org/10.2514/6.1997-2364.
[86] S. Rassou, A. Piquemal, N. Merbahi, F. Marchal, M. Yousfi, Experimental characterization of argon/air mixture microwave plasmas using optical emission spectroscopy, Journal of Molecular Spectroscopy 370 (2020) 111278. https://doi.org/https://doi.org/10.1016/j.jms.2020.111278.
[87] R. Snoeckx, R. Aerts, X. Tu, A. Bogaerts, Plasma-Based Dry Reforming: A Computational Study Ranging from the Nanoseconds to Seconds Time Scale, Journal of Physical Chemistry C 117(10) (2013) 4957-4970. https://doi.org/10.1021/jp311912b.
[88] X. Tu, B. Verheyde, S. Corthals, S. Paulussen, B.F. Sels, Effect of packing solid material on characteristics of helium dielectric barrier discharge at atmospheric pressure, Physics of Plasmas 18(8) (2011) 080702. https://doi.org/10.1063/1.3619822.

[89] F. Massines, N. Gherardi, N. Naudé, P. Ségur, Recent advances in the understanding of homogeneous dielectric barrier discharges, Eur. Phys. J. Appl. Phys. 47(2) (2009) 22805.
[90] A. Fridman, A. Chirokov, A. Gutsol, Non-thermal atmospheric pressure discharges, Journal of Physics D: Applied Physics 38(2) (2005) R1-R24. https://doi.org/10.1088/0022-3727/38/2/r01.
[91] H. Zhang, C. Du, A. Wu, Z. Bo, J. Yan, X. Li, Rotating gliding arc assisted methane decomposition in nitrogen for hydrogen production, International Journal of Hydrogen Energy 39(24) (2014) 12620-12635. https://doi.org/https://doi.org/10.1016/j.ijhydene.2014.06.047.
[92] X. Tu, L. Yu, J.H. Yan, K.F. Cen, B.G. Chéron, Dynamic and spectroscopic characteristics of atmospheric gliding arc in gas-liquid two-phase flow, Physics of Plasmas 16(11) (2009) 113506. https://doi.org/10.1063/1.3266420.
[93] F. Do Nascimento, M. Machida, M. Canesqui, S. Moshkalev, Comparison Between Conventional and Transferred DBD Plasma Jets for Processing of PDMS Surfaces, IEEE Transactions on Plasma Science PP (2017) 1-10. https://doi.org/10.1109/TPS.2017.2655266.
[94] T. Kozák, A. Bogaerts, Splitting of CO2by vibrational excitation in non-equilibrium plasmas: a reaction kinetics model, Plasma Sources Science and Technology 23(4) (2014) 045004. https://doi.org/10.1088/0963-0252/23/4/045004.
[95] A. Fridman, Plasma Chemistry, Cambridge University Press, Cambridge, 2008. https://doi.org/DOI: 10.1017/CBO9780511546075.
[96] S.Y. Moon, W. Choe, A comparative study of rotational temperatures using diatomic OH, O2 and N2+ molecular spectra emitted from atmospheric plasmas, Spectrochimica Acta Part B: Atomic Spectroscopy 58(2) (2003) 249-257. https://doi.org/https://doi.org/10.1016/S0584-8547(02)00259-8.
[97] K. Li, J.-L. Liu, X.-S. Li, X. Zhu, A.-M. Zhu, Warm plasma catalytic reforming of biogas in a heat-insulated reactor: Dramatic energy efficiency and catalyst auto-reduction, Chemical Engineering Journal 288 (2016) 671-679. https://doi.org/https://doi.org/10.1016/j.cej.2015.12.036.
[98] V. Vermeiren, A. Bogaerts, Plasma-Based CO2 Conversion: To Quench or Not to Quench?, Journal of Physical Chemistry C 124(34) (2020) 18401-18415. https://doi.org/10.1021/acs.jpcc.0c04257.
[99] R. Aerts, T. Martens, A. Bogaerts, Influence of Vibrational States on CO2 Splitting by Dielectric Barrier Discharges, Journal of Physical Chemistry C 116(44) (2012) 23257-23273. https://doi.org/10.1021/jp307525t.
[100] S. Kameshima, K. Tamura, Y. Ishibashi, T. Nozaki, Pulsed dry methane reforming in plasma-enhanced catalytic reaction, Catalysis Today 256 (2015) 67-75. https://doi.org/https://doi.org/10.1016/j.cattod.2015.05.011.

For Table of Contents Use Only